Friction **11**(7): 1292–1306 (2023)
https://doi.org/10.1007/s40544-022-0669-7
ISSN 2223-7690
CN 10-1237/TH

RESEARCH ARTICLE

Feasibility of wear reduction for soft nanostructured thin film through enhanced elastic recoverability and contact stress relief

Kuk-Jin SEO[1], **Hyun-Joon KIM**[2,3,*], **Dae-Eun KIM**[1,*]

[1] *Department of Mechanical Engineering, Yonsei University, Seoul 03722, Republic of Korea*

[2] *Department of Precision Mechanical Engineering, Kyungpook National University, Sangju 37224, Republic of Korea*

[3] *Department of Advanced Science and Technology Convergence, Kyungpook National University, Sangju 37224, Republic of Korea*

Received: 02 March 2022 / Revised: 20 May 2022 / Accepted: 23 June 2022

Abstract: This work shows that a soft, thin film comprising randomly aligned carbon nanotubes (CNTs) can reduce surface wear more effectively than a homogeneous thin film because of enhanced elastic recoverability and contact stress relief originating from its mesh structure. To investigate the wear characteristics of the mesh structure compared to those of the homogeneous thin film, multi-walled CNTs (MWCNTs) and diamond-like carbon (DLC) thin films were prepared to conduct nanoscale tribological experiments using the atomic force microscopy (AFM). The MWCNT thin film showed unmeasurably low wear compared with the DLC thin film under a certain range of normal load. To demonstrate the wear reduction mechanism of the MWCNT thin film, its indentation and frictional behaviors were assessed. The indentation behavior of the MWCNT thin film revealed repetitive elastic deformation with a wide strain range and a significantly lower elastic modulus than that of the DLC thin film. The permanent deformation of the MWCNT thin film was observed through frictional experiments under relatively high normal load conditions. These results are expected to provide insights into the design of highly wear-resistant surfaces using nanostructures.

Keywords: carbon nanotube (CNT); thin film; wear; friction; elastic recovery

1 Introduction

Numerous studies have been conducted over several decades to reduce the wear of mechanical systems [1–5]. Methods to reduce wear are generally divided into the following categories: applying lubrication, coating with high-hardness materials, and surface texturing [6–8]. Among wear reduction techniques, coating surfaces with high-hardness materials, such as diamond-like carbon (DLC), BN, WC, TiN, and Al_2O_3, are the most exploited approaches [9–11]. Thus, many researchers [12–14] have developed ultra-high hardness materials and examined their tribological characteristics. However, hard coatings eventually undergo wear despite their high hardness and potentially induce severe wear on the counter surface owing to their hard asperities and the wear debris generated from the coating [15–17]. Several studies have reported that coatings with higher hardness show more wear than those with lower hardness [18, 19]. From these reports, it is apparent that wear does not depend solely on the hardness of the surface. Hence, there is a strong motivation for utilizing additional strategies for designing wear-resistive surfaces rather than only enhancing the hardness of the coating.

Fabricating a coating with a multilayer structure is a viable wear-reduction strategy that can be readily adopted owing to recent advances in deposition technology. Amorphous carbon (a-C) has been extensively used as a material for wear-resistive multilayer coatings owing to its remarkably low friction and anti-wear characteristics [20–22]. Many

* Corresponding authors: Hyun-Joon KIM, E-mail: hjoonkim@knu.ac.kr; Dae-Eun KIM, E-mail: kimde@yonsei.ac.kr

studies [9, 21–23] reported that bonding structure including sp^3 hybridization of carbon atoms attributes chemical inertness, thermal stability, and excellent mechanical properties. In particular, DLC coatings at the micro and nanoscale have been reported to have superb tribological characteristics. Smallwood et al. [24] reported that DLC-coated microelectromechanical systems (MEMS) showed significantly improved tribological characteristics compared to the bare surface both in air and vacuum conditions. Gou et al. [25] investigated anti-wear and low adhesive characteristics of the DLC-coated atomic force microscopy (AFM) probes, reporting that the coated AFM probes showed less distorted images for a significantly longer number of measurements. Recently, there have been reported numerous studies regarding the substitution of carbon atoms with silicon, nitrogen, and transition metals to further reduce wear under various working conditions [26–29]. However, it has been observed that the ultrahigh hardness of the a-C film does not achieve superior wear resistance unless the residual stress inside the film and the elastic modulus are controlled properly [2, 20]. Many studies on a-C-based multilayer coatings have reported that the hardness to elastic modulus ratio (H/E or H^3/E^2) is one of the most critical factors for designing highly wear-resistant coatings. A high hardness to elastic modulus ratio can be achieved by inserting soft a-C layers between the hard a-C layers, which relieves the residual stress of the entire coating [30–32]. Therefore, the elasticity of the coating is critical for reducing coating wear.

To provide enhanced elasticity or damping effects, a few studies have employed nanomaterials such as carbon nanotubes (CNTs) and fullerenes. Kim et al. [33] reported a dual-layer composite coating composed of non-aligned CNTs and an Ag layer on top. The microscale tribotest results showed that the dual-layer coating had a wear rate that was over ten times lower than that of a bare silicon surface or a single Ag coating. The authors attributed the excellent wear and friction characteristics of the coating to the anchoring effect of CNTs with Ag coating, protecting the Ag layer from wear, thereby achieving low friction and the distribution of contact stress for extended sliding cycles. Yang et al. [34] demonstrated a significant reduction in wear by utilizing the C_{60} clusters underneath a DLC layer to provide nano-damping and elastic deformation when external pressure is applied. The authors stated that C_{60} clusters deformed elastically after the first few sliding cycles of the settling of C_{60} molecules. Moreover, the ductility of the overall coating was improved by utilizing its unique nanostructure. As a result, the coating exhibited a decreasing trend in the friction coefficient and reduced wear rate by two orders of magnitude. Mustafa et al. [35] investigated the tribological properties of tetrahedral a-C (ta-C) with an sp^2-rich mesh structure on top of the coating. The authors reported that the specific wear rate of mesh-structured ta-C decreased by 93% compared with that of the as-deposited ta-C because the coating was found to be more crack-resistant than the original ta-C coating. They claimed that the crack resistivity was enhanced owing to the reduced hardness of the coating, resulting in fewer brittle cracks and decreased wear debris with high hardness. Furthermore, Kim and Kim [36] proved that a nanostructured surface with optimized stiffness could minimize friction and wear by distributing contact stress through the elastic deformation of the structure. They conducted a comparative study of various corrugated nanostructures with different dimensions by using molecular dynamics simulations. The stiffness of a system can be controlled by designing a nanostructured surface. In the case of a properly designed nanostructured surface, the wear was noticeably reduced owing to elastic deformation and recovery of the nanostructure. This indicates that several mechanical characteristics should be controlled simultaneously to minimize surface wear depending on the contact sliding condition.

According to the aforementioned literature survey, wear-resistant coatings should have excellent elasticity and capability to distribute contact stress to provide further wear resistance. Specifically, wear-resistant coatings must have a high elastic strain to accommodate the deformation caused by the stress applied on the contacting asperities. However, homogeneous engineering metals or ceramics exhibit relatively low strain at the failure point. To enhance the elastic limit of a material, few studies have reported unique structures that contain porosity. By adopting the structural characteristics of a truss, three-dimensional

hollow nanostructures have been fabricated to maximize the limit of elastic strain [37–40]. In this regard, CNTs were utilized as nanomaterials to form a thin film with a mesh structure, which has the required elastic behavior to promote wear resistance [41, 42]. Owing to its anisotropic characteristics and exceptional tensile strength, it is extremely difficult to damage the nanotube in the axial direction, whereas it bends readily [43]. Therefore, nanostructured thin films composed of randomly aligned CNTs are expected to have low mechanical stiffness due to abundant voids between the nanotubes and resistance to permanent deformation owing to the superior mechanical strength of CNTs. However, there are still lacking studies on the structured film comprising CNTs with sufficient vacant space. Kim et al. [33] synthesized Ag–CNT composite coatings and reported that wear resistance was improved because of the anchoring effect of CNTs with Ag. Many studies regarding composite coatings with CNT reinforcement reported tribological improvements because the interaction between fillers and reinforcements enhanced the mechanical properties of the entire coating [44–47]. Thus, the strategy of this work is the opposite of the aforementioned literature because a nanostructure composed of CNTs only was considered to supply voids inside, decreasing the hardness and elastic modulus.

Because CNT was used in this study to fabricate the nanostructured thin film under the expectation of enhanced capability of contact stress distribution and elastic recoverability, a non-structured, homogeneous DLC thin film comprising the same element was prepared to compare tribological performance with CNT thin film. To demonstrate the wear reduction mechanism of the CNT thin film, the AFM was used to conduct nanoscale tribotests and precisely measure the wear volume.

2 Experimental setup

2.1 Specimen preparation

Si wafers were prepared as the substrates and cleaned using a piranha solution containing sulfuric acid (70%) and hydrogen peroxide (30%) [48]. A multi-walled CNT (MWCNT) suspension (JEIO, Republic of Korea) in isopropyl alcohol was used to fabricate MWCNT thin films on Si wafers via spin coating. MWCNTs were specified to have diameters of 15–25 nm and more than eight walls. Most of them were found to have lengths of 1–2 μm, and their aspect ratios were calculated to be 40–150. The 5 mL MWCNT suspension was dropped on the silicon wafer, and the wafer was rotated at a speed of 3,000 r/min.

A DLC thin film was deposited on the cleaned Si wafers by using a direct-current (DC) magnetron sputtering system (Customized model, Infovion, Republic of Korea). A graphite target was used, and the base pressure was 6.0×10^{-6} Torr. A DC of 250 mA was applied for 7,000 s under an Ar working pressure of 1.2×10^{-3} Torr.

2.2 Specimen characterization

The thickness and surface roughness of the MWCNT and DLC thin films were measured using the AFM (SPA-400, Seiko, Japan). The morphology of the MWCNT thin film was observed by the scanning electron microscopy (SEM; JSM-6610, JEOL, Japan). Nanoindentation (UNHT, Anton Paar, Austria) was performed on both MWCNT and DLC thin films using a Berkovich indenter to estimate the nano hardness and elastic modulus of each specimen. The DLC thin film was characterized using the Raman spectrometer (DXR2, Thermo Fisher Scientific, USA) to estimate the bonding composition between carbon atoms. The force–displacement (F–D) curves were measured on the MWCNT thin film using the AFM to verify the mechanical behavior when indented by the zirconia microspheres that were used for wear and friction experiments. The adhesion forces between the thin films and zirconia microspheres were measured by observing the pull-off force of the F–D curve with the AFM. The adhesion force was measured using a colloidal AFM probe to aid the analysis of the tribological characteristics of the thin film. The pull-off forces for the DLC specimens were obtained at 35 different locations with displacements of 50–200 nm. Diamond-coated AFM probes (DT-NCHR, NanoWorld, Switzerland) were used for scanning, while non-coated silicon AFM probes with relatively high and low spring constants (NCHR and CONTR, NanoWorld, Switzerland) were used for the tribological experiments and specimen characterizations.

2.3 Experimental procedure

Prior to the wear and friction experiments, the normal spring constants of the AFM probe cantilevers were calibrated using the Sader method [49]. The AFM probe cantilevers with relatively low spring constants (~0.2 N/m) were used to apply low normal loads of less than 500 nN, whereas cantilevers with relatively high spring constants (~40 N/m) were used to apply higher normal loads of over 500 nN. Yttria-stabilized zirconia microspheres (diameter of ~31 μm) were employed instead of the bare AFM tips as the counter surfaces to prevent severe wear of the tip because the nano hardness of yttria-stabilized zirconia crystals was reported to be approximately 20 GPa [50]. Since zirconia is also reported to be chemically inert, it was expected that the chemical reaction with the thin films would be negligible during the tribological experiments [51]. The microspheres were attached to the end of the AFM probe cantilevers using an ultraviolet (UV) epoxy adhesive, as shown in Fig. 1. The microsphere-attached AFM probes (colloidal probes) were cured under UV light for 24 h.

Wear experiments were conducted in the following three steps: (1) measurement of the surface topography of the pristine specimens, (2) wear test under a constant normal load, and (3) measurement of the surface topography of the wear track. For the surface measurements (steps (1) and (3)), a noncontact (tapping) mode was used to prevent surface damage. Through a series of pretests, the suitable normal load, stroke, reciprocating cycles, and linear sliding speed for the wear test were determined to be 700–28,000 nN, 10–20 μm, 1,000–30,000 cycles, and 12 μm/s, respectively. Because the maximum depth of the wear tracks on the surfaces was a few tens of nanometers, it was necessary to consider the surface roughness to accurately calculate the wear volume. Thus, the surface image of the MWCNT specimens with the wear track was processed by subtracting the image measured before the test to obtain the accurate geometry of the wear track. To quantitatively analyze the wear characteristics under different test conditions, the wear rate was obtained by dividing the wear volume (mm^3) by the normal load (N) and total sliding distance (mm) [20]. After conducting all the experiments, the wear rates were calculated using the wear volume measurements for each experiment.

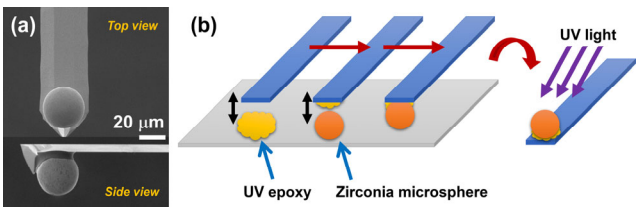

Fig. 1 (a) SEM images of zirconia microsphere-attached (diameter of 31 μm) AFM cantilever and (b) schematic of the method for attaching the microsphere to the end of the AFM cantilever.

Friction experiments were conducted with normal loads of 50–8,000 nN, stroke of 20 μm, and linear speed of 20 μm/s for the initial 30 cycles to compare the frictional behaviors of the MWCNT and DLC thin films under each normal load condition. The number of sliding cycles was determined to obtain initial frictional characteristics with minimal surface wear. The ratio of the friction signals of the MWCNT and DLC thin films under identical normal loads was calculated. Additional experiments with normal loads of 5,000 and 20,000 nN for 500 cycles were performed to investigate the relationship between the wear of the MWCNT thin film and the frictional signal.

3 Results and discussion

3.1 Specimen characteristics

The thicknesses of the MWCNT and DLC thin films were approximately 800 and 440 nm, respectively. The MWCNT thin film was determined to be sufficiently thick to avoid the substrate effect when deformed, considering its low elastic modulus. The thickness of the DLC thin film was determined to avoid delamination owing to the internal stress that developed during the deposition process. It was postulated that the difference in thickness between the films would not affect their tribological characteristics, because both thin films were sufficiently thick to avoid the substrate effect. The average surface roughnesses (R_a) of each thin film were ~100 nm (MWCNT) and 1.0 nm (DLC), as shown in Figs. 2(a) and 2(b), respectively. The relatively high roughness of the MWCNT thin film was attributed to several protruding nanotubes on the surface with low bending stiffness; therefore, they were not considered to be hard asperities [41, 43]. The morphology of the MWCNT thin film

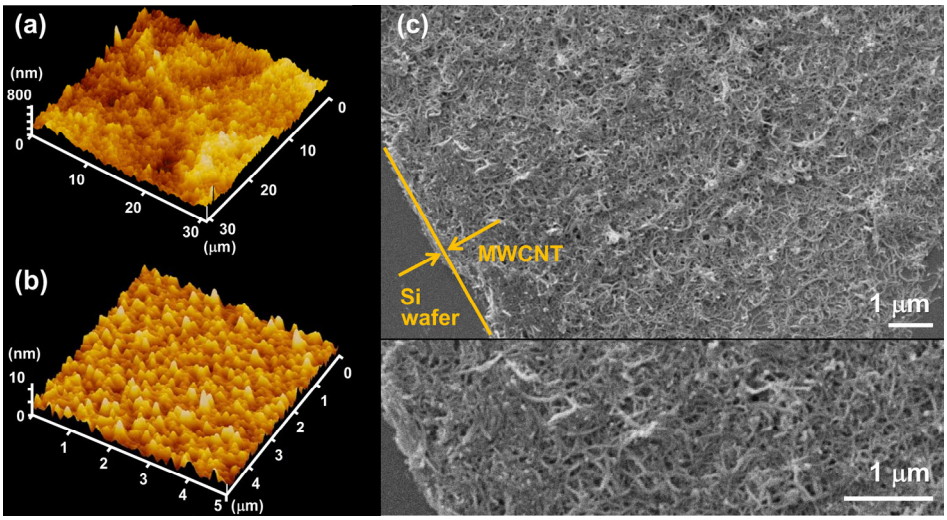

Fig. 2 AFM images for the measurement of average surface roughness of (a) MWCNT (~100 nm) and (b) DLC (1.0 nm) thin films. (c) SEM image of MWCNT thin film surface.

was a mesh structure consisting of randomly entangled MWCNTs with voids. The mesh structure of the MWCNT thin film was revealed by using the SEM (Fig. 2(c)). Owing to the high aspect ratio of CNTs, the porous mesh structure was expected to exhibit low stiffness, although a single nanotube itself has excellent strength and elasticity in the axial direction [52].

The nanoindentation results with the Berkovich indenter are shown in Figs. 3(a) and 3(b). The F–D curves were measured at over eight different locations for each thin film and then averaged. The F–D curves were obtained at a loading/unloading rate of 50 μN/min, maximum load of 100 μN, and pause time of 600 s for the MWCNT thin film; loading/unloading rate of 200 μN/min and maximum load of 400 μN for the DLC thin film. The nanoindentation conditions were determined by considering the stability and repeatability of the data with the minimum substrate effect. The nano hardness of MWCNT and DLC thin films were calculated to be 95.2±23.3 MPa and 13.7±1.5 GPa with the maximum indentation depths of 208±16 and 37±1 nm, respectively. The elastic moduli of the MWCNT and DLC thin films were 4.3±0.8 and 172.3± 18.0 GPa, respectively. The nano hardness and elastic modulus of MWCNT were found to be 144-fold and 40-fold lower than those of DLC, respectively. The nanoindentation result of DLC thin film is in the accordance with the results reported by Vetter [22] and Valencia et al. [53]. In the case of MWCNT thin film, Koumoulos and Charitidis [54] measured the mechanical behavior of vertically aligned MWCNT using nanoindentation and reported the nano hardness and elastic modulus of in-between area MWCNT as ~10 MPa and ~10 GPa, respectively. Though the structure of MWCNT is significantly different from that of MWCNT in this work, the orders of magnitude of hardness and modulus are similar to those in this work.

The Raman peak shift result of MWCNT thin film is shown in Fig. 3(c). The result is commensurate with that reported previously for the MWCNT [55].

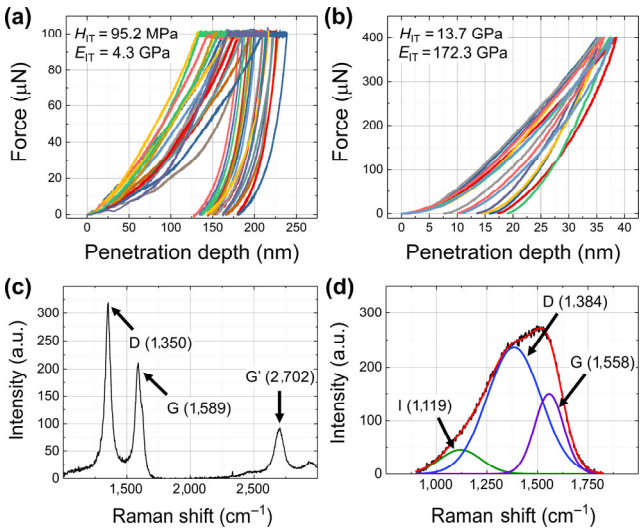

Fig. 3 Nanoindentation measurement results of (a) MWCNT and (b) DLC thin films and their average nano hardness (H_{IT}) and elastic modulus (E_{IT}). Raman spectrum measurement results of (c) MWCNT and (d) DLC thin films.

The Raman peak shift analysis for DLC thin film is shown in Fig. 3(d). The I peak originates from either sp^2 bonding of transpolyacetylene segments at the boundaries or the stretching of CH or sp^3 bonding in the a-C structure [56]. The I, D, and G peaks were observed at 1,119, 1,384, and 1,558 cm^{-1}, respectively, with a full width at half maximum of 240, 316, and 168 cm^{-1}, respectively [57, 58]. The intensity ratio of the D to G peaks (I(D)/I(G)) was calculated as 1.57, which indicated an sp^3 content estimation of approximately 30% [59].

Indentation tests for displacement were conducted for the MWCNT thin film by using the AFM colloidal probes, as shown in Figs. 4(a)–4(d). Because the nominal displacement indicated in Fig. 4 includes the deflection of the AFM probe cantilever, the actual indentation depths on the MWCNT thin film were less than the nominal values. Though there were found subtle hysteretic behaviors and experimental uncertainties in the F–D curve data, the elastic behaviors could be successfully observed based on the values indicating contact or detachment. A slight permanent deformation of the MWCNT thin film was observed at the first indentation during the repeated indentation tests, as shown in Fig. 4. Ideally, the loading and unloading graphs should be identical if a permanent deformation does not occur. However, those obtained at the first indentation exhibited different displacements, at which the normal load became zero, indicating that the probe was attached to or detached from the surface at different heights. As shown in Fig. 4(b), the difference was approximately 10 nm. However, the F–D curves obtained from the second to fifth tests were approximately identical. The displacements of the zero normal load of the data in the loading and unloading processes were not significantly different; that is, there was no permanent deformation. The slight difference between them was regarded as experimental uncertainty and measurement noise. Hence, permanent deformation of the MWCNT thin film occurred only at the first indentation, and elastic deformation was the primary mechanical behavior for the rest of the indentation tests. Additional F–D curves were obtained by indenting the thin film up to a nominal displacement of 750 nm, which corresponds to the measurement limit of the AFM

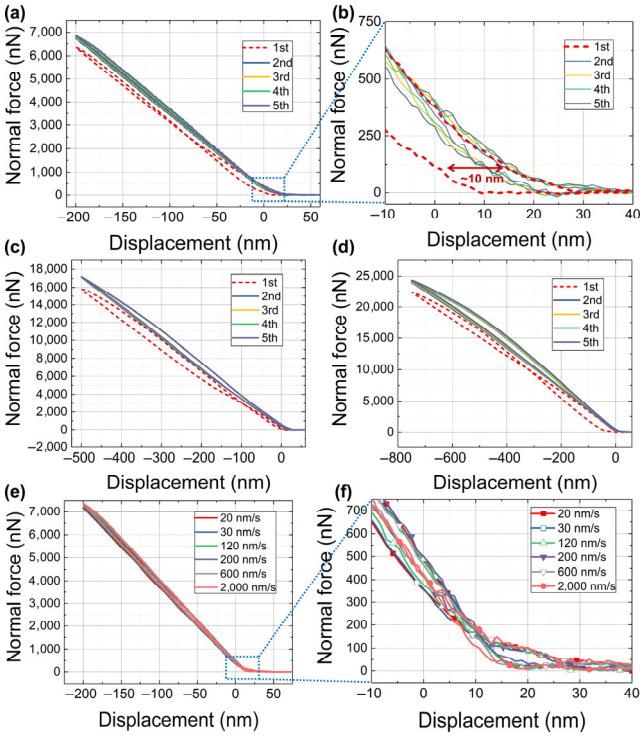

Fig. 4 (a) F–D curves with five repeated indentation tests with a displacement of 200 nm at the same point on the MWCNT thin film and (b) its magnified graph near the contact points. F–D curves with displacements of (c) 500 nm and (d) 750 nm. (e) F–D curves with various indentation speeds from 20 to 2,000 nm/s and (f) its magnified graph near the contact points.

probe cantilever. Figures 4(c) and 4(d) show the F–D curves with the nominal displacements of 500 and 750 nm, respectively. The results indicate that the MWCNT thin film exhibited no permanent deformation, except for a subtle deformation at the first indentation, up to a nominal displacement of 750 nm. Strain could be calculated simply by dividing the deformation of the thin film excluding the deflection of the cantilever by the total thickness of the film. The strain at this maximum displacement was calculated to be ~5.5%, excluding the deflection of the AFM probe cantilever. It was found that the MWCNT thin film deformed elastically when indented with a normal load of up to ~24,000 nN.

It was presumed that the as-fabricated MWCNT thin film had a loose structure. When external compressive stress was applied, the alignment of the nanotubes located at the surface and the subsurface of the film was altered until the van der Waals force between the nanotubes and the recovery force against the bending of the nanotubes became balanced,

forming a less porous surface. Thus, the thickness of the MWCNT thin film was slightly reduced from its original state [41]. In addition, to assess the effect of the indentation speed, repeated indentation tests were conducted at various speeds (from 20 to 2,000 nm/s). As shown in Figs. 4(e) and 4(f), the indentation speed did not affect the mechanical behavior of the MWCNT thin films. The results showed that the MWCNT thin film was not permanently deformed and behaved as an elastic film when indented at a speed of less than 2,000 nm/s.

The adhesion force between the DLC thin film and the zirconia microsphere was obtained by measuring the pull-off force when indenting and unloading the microsphere on the specimen surface. The average adhesion force between the DLC and microspheres was calculated to be 1,186 nN with a standard deviation of 80 nN. For the MWCNT thin film, the pull-off force could not be measured, as shown in Fig. 4(b). The adhesion force between the MWCNT thin film and the colloidal probe was unmeasurably low because the spring constant of the probe cantilever was relatively high; therefore, it was not sufficiently sensitive to measure the nanoscale pull-off force. In addition, the adhesion force with the microsphere was presumed to be higher for the DLC thin film owing to its lower surface roughness than that of MWCNTs, resulting in greater contact area.

3.2 Tribological characteristics

Wear tests were conducted on MWCNT and DLC thin films under various normal loads and sliding cycles. The wear tests under high normal loads were conducted with fewer sliding cycles that could induce evident wear tracks on the specimen surfaces than those under low normal loads to avoid additional unnecessary wear by three-body abrasion. Figure 5 shows the wear rate results of each specimen with respect to the normal load. Both thin films showed an increasing trend in wear rate with the increasing normal load. The wear rate results of the DLC thin film were approximately one order of magnitude lower than those of the MWCNTs, except for the results with normal loads of less than 7,000 nN for the MWCNT thin film. The wear rate in the order of 10^{-8} $mm^3/(N{\cdot}mm)$ for the DLC thin film seemed to be in accordance with the previous literature by Al Mahmud et al. [60] and Chung and Kim [61] considering the experimental scale. The wear rate marked as zero for the MWCNT thin film with a normal load of less than 7,000 nN indicates that it was not able to detect wear tracks on the surface.

From the results, the most prominent phenomenon was that the wear was not measurable on the MWCNT specimen with the AFM scan under normal load conditions lower than 7,000 nN and up to 30,000 sliding cycles. Although the AFM image, where the wear track was expected to be located, was post-processed by subtracting the original image before the test, measurable wear did not occur under these conditions. Figures 6(a)–6(c) show the images after the wear tests on the MWCNT thin film under 20,000 and 30,000 sliding cycles and normal loads of 2,000, 6,000, and 7,000 nN. Figures 6(g)–6(i) show the post-processed images obtained by subtracting the original image before the test from the image after the test. Although some irregularities remained after the process owing to the noise and drift during the scan, there was no evidence of wear in the images with a normal load of less than 7,000 nN (Figs. 6(g) and 6(h)). It could be considered that there was no practical wear, even though the post-process removed most of the roughness from the surface. The unmeasurably low wear is attributed to the fact that the MWCNT thin film was elastically deformed when indented, as shown in the series of F–D curve measurements. In this case, it was considered that the normal load was distributed to more nanotubes because of the low elastic modulus, and the contact stress applied to the individual nanotubes was not excessively high to alter the arrangement of the mesh structure. Thus, the MWCNT thin film did not wear out practically under these conditions.

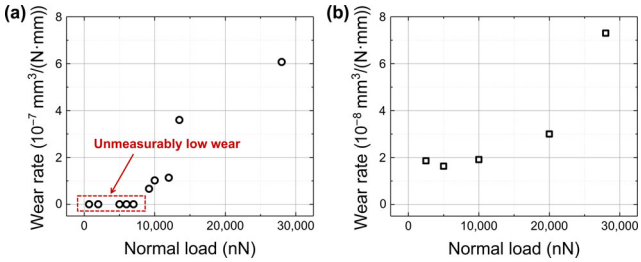

Fig. 5 Wear rates of (a) MWCNT and (b) DLC thin films with respect to a normal load of up to 28,000 nN.

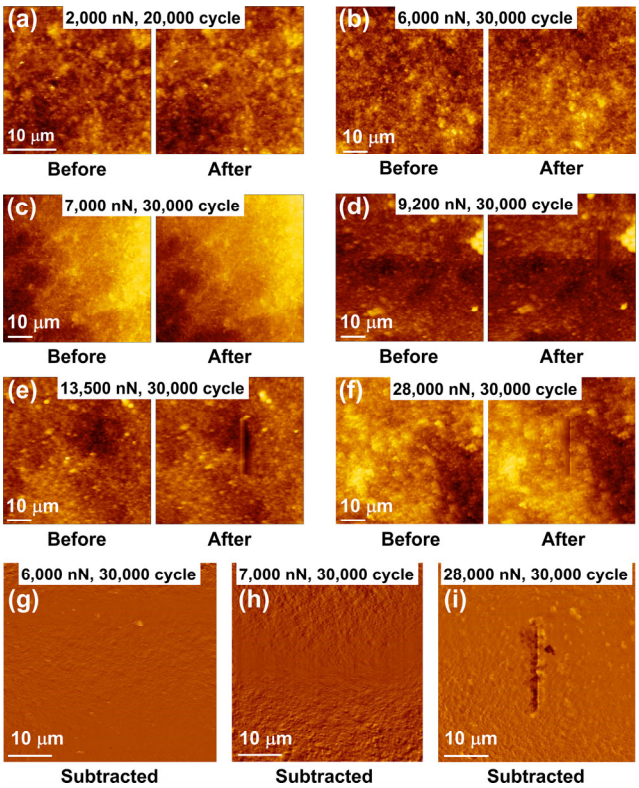

Fig. 6 AFM images of wear tracks on the MWCNT thin film under test conditions of (a) 2,000 nN and 20,000 cycles, (b) 6,000 nN and 30,000 cycles, (c) 7,000 nN and 30,000 cycles, (d) 9,200 nN and 30,000 cycles, (e) 13,500 nN and 30,000 cycles, and (f) 28,000 nN and 30,000 cycles. Post-processed AFM images that subtracted the original image before each wear test under conditions of (g) 6,000 nN and 30,000 cycles, (h) 7,000 nN and 30,000 cycles, and (i) 28,000 nN and 30,000 cycles.

For the wear test results with normal loads of over 7,000 nN, the MWCNT thin film showed evident wear, as shown in Figs. 6(d)–6(f). The processed image (Fig. 6(i)) also showed an evident wear track. Because the MWCNT thin film has an elastic modulus approximately 40-fold lower than that of DLC, the nanotubes inside the film experienced higher deformation when compressed; therefore, the shear stress induced by the movement of the counter microsphere influenced more nanotubes in contact. At this point, the mesh structure of the MWCNT thin film was presumed to be permanently deformed by rearranging the structure rather than the destruction of the nanotubes because the bonding between MWCNTs comprised weak van der Waals forces and their intermolecular shear strength was reported to be significantly lower than the bending or compressive strength [62–66]. Figure 7 shows the frictional signals averaged over the initial 30 cycles of each thin film and their ratios with respect to the normal load. Under low normal load conditions, the frictional signals of the MWCNT thin film were significantly lower than those of DLC (Fig. 7(b)), whereas the signals considerably increased as the normal load increased (Fig. 7(f)). In this regard, as the normal load increased, the excessive shear stress induced by the increased friction was postulated to result in the permanent deformation of the MWCNT thin film.

The wear rate of the MWCNT thin films increased rapidly with the increasing normal load. Because the elastic modulus of the MWCNT thin film is considerably lower than that of the DLC film, the mesh structure deformed easily, and the number of junctions between the nanotubes that supported the external normal load possibly increased under high normal load conditions to support the corresponding normal load. Thus, the possibility of permanent deformation increased during sliding. Figure 8 shows

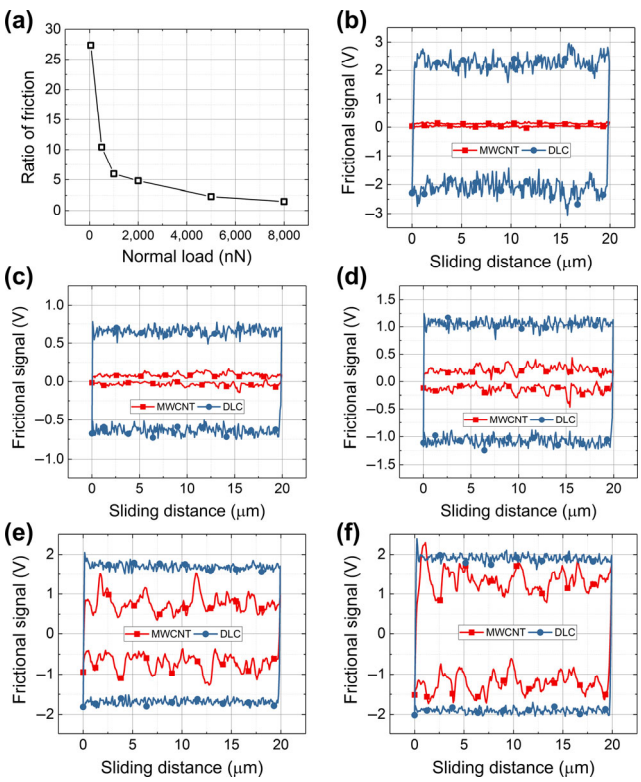

Fig. 7 (a) Frictional signal ratios of the DLC to the MWCNT thin film with respect to normal loads and (b–f) averaged friction signals of each thin film with normal loads of 50, 500, 1,000, 5,000, and 8,000 nN. Each friction signal was averaged over 30 cycles of friction tests.

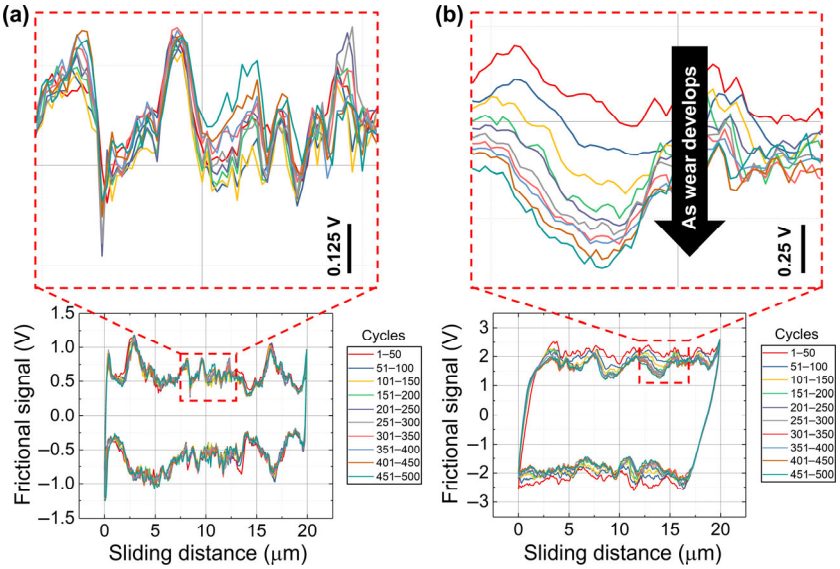

Fig. 8 Frictional signals with respect to sliding cycles under normal loads of (a) 5,000 nN and (b) 20,000 nN. Each line indicates the averaged signal value of 50 cycles in sequence up to 500 cycles.

the evidence of the permanent deformation of the MWCNT thin film with respect to the sliding cycles under a high normal load condition (20,000 nN) compared to the deformation behavior under a low normal load condition (5,000 nN). In Fig. 8(a), the frictional signal did not show a significant difference under a low normal load (5,000 nN) as the number of cycles increased because the morphology of the thin film did not change during the test. Thus, it appeared that the nanotubes were elastically deformed and immediately restored under this normal load condition, as illustrated in Fig. 9(a). However, as shown in Fig. 8(b) (normal load of 20,000 nN), the frictional signal consistently decreased as the number of cycles increased. This is because the morphology of the MWCNT thin film changed with an increasing number of sliding cycles. The change in the morphology is attributed to the decrease in the number of nanotubes in front of the microsphere owing to the permanent deformation that occurred in the previous sliding cycles, as illustrated in Fig. 9(b). Permanent deformation accumulated over the cycles, resulting in a consistently decreasing frictional signal (Fig. 8(b)). Considering that the F–D curve results, as described in Section 3.1, showed elastic behaviors under the same normal loads of 5,000 and 20,000 nN, the permanent deformation

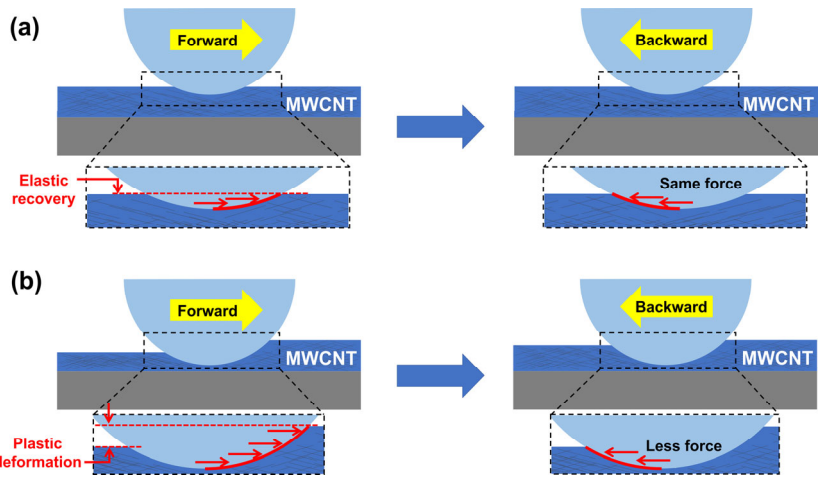

Fig. 9 Schematics describing the difference in the frictional behavior of MWCNT thin film under (a) low and (b) high normal load conditions.

displayed in Fig. 8(b) was difficult to understand. The only difference between the F–D curve experiment and the friction test was the horizontal motion of the microspheres. Thus, the shear stress exerted on the thin film induced by the friction force was regarded as the reason for the permanent deformation of the MWCNT thin film.

In contrast, the DLC thin film was distinctly worn out under normal loads of less than 7,000 nN, as shown in Figs. 10(a) and 10(b). This result is attributed to the fact that DLC is a homogeneous material with limited yield strength, and that counter microspheres have higher hardness [50, 67, 68]. Although the nominal contact pressure is lower than the yield strength or hardness of the DLC material, the actual contact starts from asperities existing on the surface. Thus, the real contact pressure and shear stress exerted by the counter microsphere could exceed the material's limitation, resulting in plastic deformation and abrasive wear by plowing [69]. In addition, as described in Section 3.1, the surface was more susceptible to wear than the MWCNT surface because the DLC thin film showed a significant adhesion force with the counter microsphere. For normal loads higher than 7,000 nN, a rapid increase in wear rate was observed, as shown in Figs. 10(c) and 10(d). Nevertheless, the wear rates of DLC thin films with a high normal load of over 7,000 nN were still lower than those of MWCNT thin films owing to the prominent wear resistance reported by numerous researchers [9, 21, 70]. In contrast, under normal loads of less than 7,000 nN, the wear test results showed that there was unmeasurably low wear on the MWCNT thin film, although the sliding cycles were significantly higher than those for the DLC thin film. It was confirmed that the MWCNT thin film had feasibility of exceptional wear resistance compared with DLC under a certain range of normal load conditions. Frictional experiments were conducted to investigate the superior wear resistance of the MWCNT thin film under a certain range of normal loads.

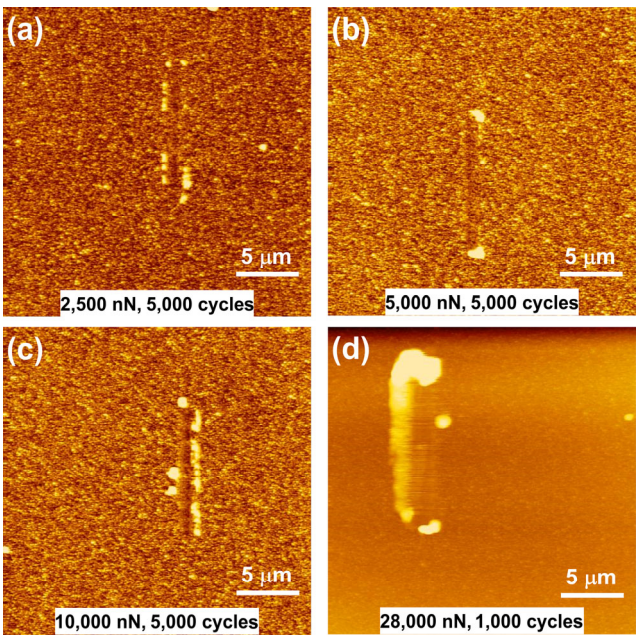

Fig. 10 AFM images of wear track on the DLC thin film after wear tests under conditions of (a) 2,500 nN and 5,000 cycles, (b) 5,000 nN and 5,000 cycles, (c) 10,000 nN and 5,000 cycles, and (d) 28,000 nN and 1,000 cycles.

The frictional signals show a significant difference between the MWCNT and DLC thin films (Fig. 7). As shown in Fig. 7(a), the average frictional signals of the MWCNT thin film were 27.4- and 1.5-fold lower than those of the DLC thin film under normal loads of 50 and 8,000 nN, respectively. On the contrary to the DLC thin film, the frictional characteristics of the MWCNT thin film seemed to be highly dependent on the deformation by the normal load owing to its low elastic modulus and hardness. Because the mesh structure of the MWCNT thin film has a significantly discontinuous contact area originating from abundant empty spaces between the nanotubes, the real contact area with the counter surface seemed to be considerably smaller than that of DLC under the same low normal load conditions. The measurement results showed that the adhesion force of the MWCNT thin film was unmeasurably low (Section 3.1), which could be explained by the same mechanism. In addition, the force required to deform the nanotubes in front of the counter microsphere was lower than that under higher normal load conditions because the number of nanotubes deformed by the lower normal load was smaller. Thus, the frictional signal of MWCNT thin film was exceptionally lower than that of the DLC thin film because of the low deformation, real contact area, and adhesion force at the low normal load of 50 nN. However, when the normal load was increased to 8,000 nN, the discrepancy in the frictional signal

between the thin films decreased. The larger number of nanotubes at the surface of the MWCNT thin film started to contact the counter microsphere to support a higher normal load. Thus, the microsphere required a higher force to deform the nanotubes in front of its motion. As the frictional signal of the MWCNT thin film developed significantly, the ratio of frictional signals of the DLC to the MWCNT thin film decreased to 1.5-fold from 27.4-fold as the normal load increased from 50 to 8,000 nN.

The MWCNT and DLC thin films exhibited different wear characteristics. In the case of the MWCNT thin film, the wear tracks were mostly concave without wear burrs or particles surrounding them (Figs. 6(d)–6(f)). Because the mesh structure of the MWCNT thin film included abundant vacant space, the nanotubes were presumed to be bent and rearranged to fill the space rather than protrude outward. This phenomenon is attributed to the low intermolecular shear strength due to the weak van der Waals interaction between the nanotubes [62]. Hwang et al. [41] reported similar results that the surface roughness of a randomly aligned CNT thin film was decreased when compressed with a flat counter surface because of the deformation of protruded nanotubes on the surface. Thus, the nanotubes near the surface could be permanently deformed to densify the mesh structure and reduce the protrusion on the surface when the compressive and shear stresses were applied. However, the wear tracks of the DLC thin film consistently showed burrs and wear particles at the end or along the tracks (Fig. 10). Compared to the MWCNTs, the DLC thin film consists of a homogeneous structure of carbon atoms; therefore, its wear process produces burrs and wear particles.

4 Conclusions

The AFM experiments were conducted to demonstrate the tribological benefits of the MWCNT thin film with mesh structures, based on its elastic recoverability and contact stress distribution at the nanoscale, compared to the homogeneous DLC thin film. To demonstrate that the MWCNT thin films have superior wear resistance under certain conditions owing to their elasticity based on their nanostructure, mechanical and tribological characteristics were investigated. To confirm the elasticity, F–D curve measurements were performed by indenting and unloading the specimens using a colloidal AFM probe. The nano hardness and elastic modulus of each thin film were further characterized by using the nanoindentation technique. Wear experiments were conducted to quantitatively evaluate the wear rate of each specimen under various experimental conditions of sliding cycles and normal loads. Frictional experiments were conducted to investigate the wear mechanism of MWCNT thin films under various normal load conditions. Based on the results obtained in this work, the following conclusions were deduced:

1) The nanoindentation results showed that the nano hardness and elastic modulus of MWCNT thin film were 95.2 MPa and 4.3 GPa, respectively. These values were considerably lower than those of DLC thin film (nano hardness of 13.7 GPa and elastic modulus of 172.3 GPa). This result was attributed to the mesh structure of the MWCNT thin film, which comprised entangled nanotubes with abundant voids. In addition, the MWCNT thin film showed repetitive elasticity even when indented with a normal load of ~24,000 nN at an indentation speed of less than 2,000 nm/s in the F–D curve measurements by using the AFM.

2) The results of the wear experiments showed that wear tracks were not measurable for the MWCNT thin film with a normal load of less than 7,000 nN and sliding cycles of up to 30,000. The unmeasurably low wear was attributed to the elastic deformation and contact stress distribution of the MWCNT thin film. In contrast, the DLC thin film was readily worn out, at a much lower normal load of 2,500 nN, within 5,000 sliding cycles.

3) With an increase in the normal load over 7,000 nN, the wear rate of both thin films showed an increasing trend. For the MWCNT thin film, the normal and shear stress induced by the load and sliding motion of the counter surface were presumed to exceed the intermolecular shear strength to permanently deform the mesh structure. For the DLC thin film, the higher normal load caused stress concentration owing to its high hardness and elastic modulus, resulting in plastic deformation and abrasive wear by plowing.

4) The frictional experiments conducted for the sliding cycles demonstrated evidence of the elastic recoverability and permanent deformation of the MWCNT thin film during the tests. With a low normal load of 5,000 nN, the frictional signal did not change significantly as the number of sliding cycles increased, proving that there was no practical wear. However, with a high normal load of 20,000 nN, the frictional signal decreased as the number of sliding cycles increased because the thin film experienced accumulative permanent deformation through the previous cycles; thus, the counter microsphere needed less force to deform the nanotubes than the previous cycles.

Acknowledgements

This work was supported by the National Research Foundation of Korea (NRF) grant funded by the Korean government (MSIT) (No. 2020R1A2C2004714). This work was also supported by Basic Science Research Program through the National Research Foundation of Korea (NRF) funded by the Ministry of Education (No. 2021R1I1A3060608).

Declaration of competing interest

The authors have no competing interests to declare that are relevant to the content of this article.

References

[1] Holmberg K, Erdemir A. The impact of tribology on energy use and CO_2 emission globally and in combustion engine and electric cars. *Tribol Int* **135**: 389–396 (2019)

[2] Khadem M, Penkov O V, Yang H K, Kim D E. Tribology of multilayer coatings for wear reduction: A review. *Friction* **5**(3): 248–262 (2017)

[3] Kim H J, Yoo S S, Kim D E. Nano-scale wear: A review. *Int J Precis Eng Manuf* **13**(9): 1709–1718 (2012)

[4] Kim H J, Seo K J, Kang K H, Kim D E. Nano-lubrication: A review. *Int J Precis Eng Manuf* **17**(6): 829–841 (2016)

[5] Lee H Y. Sliding wear behavior of carbon steel in changing sliding speed (effects of mild wear mode test on subsequent severe wear behavior). *Tribol Lubr* **36**(3): 117–123 (2020) (in Korean)

[6] Farfan-Cabrera L I. Tribology of electric vehicles: A review of critical components, current state and future improvement trends. *Tribol Int* **138**: 473–486 (2019)

[7] Rosenkranz A, Costa H L, Baykara M Z, Martini A. Synergetic effects of surface texturing and solid lubricants to tailor friction and wear—A review. *Tribol Int* **155**: 106792 (2021)

[8] Khawaja A U H, Jahanzaib M, Munawar M. Optimizing the performance of high-speed machining on 15CDV6 HSLA steel in terms of green manufacturing using response surface methodology and artificial neural network. *Int J Precis Eng Manuf* **22**(6): 1125–1145 (2021)

[9] Erdemir A, Martin J M. Superior wear resistance of diamond and DLC coatings. *Curr Opin Solid State Mater Sci* **22**(6): 243–254 (2018)

[10] Gu Y Q, Xia K, Wu D H, Mou J G, Zheng S H. Technical characteristics and wear-resistant mechanism of nano coatings: A review. *Coatings* **10**(3): 233 (2020)

[11] Wu T T, Li Y F, Liu G J, Zhao H Y, Wu B L. Effect of Yb_2O_3 and Tm_2O_3 on the wear resistance of high-alumina ceramics. *Wear* **452–453**: 203281 (2020)

[12] Bai H Q, Zhong L S, Kang L, Liu J B, Zhuang W J, Lv Z L, Xu Y H. A review on wear-resistant coating with high hardness and high toughness on the surface of titanium alloy. *J Alloys Compd* **882**: 160645 (2021)

[13] Amanov A, Sasaki S. A study on the tribological characteristics of duplex-treated Ti–6Al–4V alloy under oil-lubricated sliding conditions. *Tribol Int* **64**: 155–163 (2013)

[14] Abdul Halim N H, Che Haron C H, Abdul Ghani J. Sustainable machining of hardened inconel 718: A comparative study. *Int J Precis Eng Manuf* **21**(7): 1375–1387 (2020)

[15] Kato K, Adachi K. Wear of advanced ceramics. *Wear* **253**(11–12): 1097–1104 (2002)

[16] Lee H G, Hwang H Y, Lee D G. Effect of wear debris on the tribological characteristics of carbon fiber epoxy composites. *Wear* **261**(3–4): 453–459 (2006)

[17] Gheisari R, Polycarpou A A. Three-body abrasive wear of hard coatings: Effects of hardness and roughness. *Thin Solid Films* **666**: 66–75 (2018)

[18] Kato K. Wear in relation to friction—A review. *Wear* **241**(2): 151–157 (2000)

[19] Bhushan B, Galasso B, Bignardi C, Nguyen C V, Dai L M, Qu L T. Adhesion, friction and wear on the nanoscale of MWNT tips and SWNT and MWNT arrays. *Nanotechnology* **19**(12): 125702 (2008)

[20] Penkov O V, Devizenko A Y, Khadem M, Zubarev E N, Kondratenko V V, Kim D E. Toward zero micro/macro-scale wear using periodic nano-layered coatings. *ACS Appl Mater Interfaces* **7**(32): 18136–18144 (2015)

[21] Tyagi A, Walia R S, Murtaza Q, Pandey S M, Tyagi P K, Bajaj B. A critical review of diamond like carbon coating for wear resistance applications. *Int J Refract Met Hard Mater* **78**: 107–122 (2019)

[22] Vetter J. 60 years of DLC coatings: Historical highlights and technical review of cathodic arc processes to synthesize various DLC types, and their evolution for industrial applications. *Surf Coat Technol* **257**: 213–240 (2014)

[23] Meng Y G, Xu J, Jin Z M, Prakash B, Hu Y Z. A review of recent advances in tribology. *Friction* **8**(2): 221–300 (2020)

[24] Smallwood S A, Eapen K C, Patton S T, Zabinski J S. Performance results of MEMS coated with a conformal DLC. *Wear* **260**(11–12): 1179–1189 (2006)

[25] Gou L Q, Shi X L, Zhao X M, Bai Y, Qiao L J. Composite diamond-DLC coated nanoprobe tips for wear resistance and adhesion reduction. *Surf Coat Technol* **206**(19–20): 4099–4105 (2012)

[26] Zhou Y F, Li L L, Shao W, Chen Z H, Wang S F, Xing X L, Yang Q X. Mechanical and tribological behaviors of Ti–DLC films deposited on 304 stainless steel: Exploration with Ti doping from micro to macro. *Diam Relat Mater* **107**: 107870 (2020)

[27] Patnaik L, Maity S R, Kumar S. Comprehensive structural, nanomechanical and tribological evaluation of silver doped DLC thin film coating with chromium interlayer (Ag–DLC/Cr) for biomedical application. *Ceram Int* **46**(14): 22805–22818 (2020)

[28] Zhang T F, Wan Z X, Ding J C, Zhang S H, Wang Q M, Kim K H. Microstructure and high-temperature tribological properties of Si-doped hydrogenated diamond-like carbon films. *Appl Surf Sci* **435**: 963–973 (2018)

[29] Kong C C, Guo P, Sun L L, Zhou Y, Liang Y X, Li X W, Ke P L, Lee K R, Wang A Y. Tribological mechanism of diamond-like carbon films induced by Ti/Al co-doping. *Surf Coat Technol* **342**: 167–177 (2018)

[30] Lin Y Y, Zia A W, Zhou Z F, Shum P W, Li K Y. Development of diamond-like carbon (DLC) coatings with alternate soft and hard multilayer architecture for enhancing wear performance at high contact stress. *Surf Coat Technol* **320**: 7–12 (2017)

[31] Jang Y J, Kim J I, Lee W, Kim J. Tribological properties of multilayer tetrahedral amorphous carbon coatings deposited by filtered cathodic vacuum arc deposition. *Friction* **9**(5): 1292–1302 (2021)

[32] Wei J, Li H C, Liu L L, Guo P, Ke P L, Wang A Y. Enhanced tribological and corrosion properties of multilayer ta-C films via alternating sp^3 content. *Surf Coat Technol* **374**: 317–326 (2019)

[33] Kim D E, Kim C L, Kim H J. A novel approach to wear reduction of micro-components by synthesis of carbon nanotube–silver composite coating. *CIRP Ann-Manuf Techn* **60**(1): 599–602 (2011)

[34] Yang H K, Khadem M, Penkov O V, Kim D E. Increased elasticity and damping capacity of diamond-like carbon coatings by immobilized C_{60} fullerene clusters. *Nanoscale* **11**(6): 2863–2870 (2019)

[35] Mustafa M M B, Umehara N, Tokoroyama T, Murashima M, Shibata A, Utsumi Y, Moriguchi H. Effect of mesh structure of tetrahedral amorphous carbon (ta-C) coating on friction and wear properties under base-oil lubrication condition. *Tribol Int* **147**: 105557 (2020)

[36] Kim H J, Kim D E. Wear minimization through utilization of atomic-scale functional surface structure. *Appl Phys Lett* **103**(15): 151904 (2013)

[37] Kim H, Yun S, Kim K, Kim W, Ryu J, Nam H G, Han S M, Jeon S, Hong S. Breaking the elastic limit of piezoelectric ceramics using nanostructures: A case study using ZnO. *Nano Energy* **78**: 105259 (2020)

[38] Na Y E, Shin D, Kim K, Ahn C, Jeon S, Jang D. Emergence of new density-strength scaling law in 3D hollow ceramic nanoarchitectures. *Small* **14**(44): 1802239 (2018)

[39] Li X Y, Gao H J. Smaller and stronger. *Nat Mater* **15**(4): 373–374 (2016)

[40] Tan H, Yu X Z, Huang K, Zhong J X, Lu B G. Large-scale *carambola*-like V_2O_5 nanoflowers arrays on microporous reed carbon as improved electrochemical performances lithium-ion batteries cathode. *J Energy Chem* **51**: 388–395 (2020)

[41] Hwang Y H, Myung B S, Kim H J. Study on frictional behavior of carbon nanotube thin films with respect to surface condition. *Friction* **6**(4): 432–442 (2018)

[42] Kim H J, Kim C L. Effect of nanomesh structure variation on the friction and wear characteristics of carbon nanotube coatings. *Tribol Lubr* **36**(6): 315–319 (2020) (in Korean)

[43] Coleman J N, Khan U, Blau W J, Gun'ko Y K. Small but strong: A review of the mechanical properties of carbon nanotube-polymer composites. *Carbon* **44**(9): 1624–1652 (2006)

[44] Lei J B, Shi C, Zhou S F, Gu Z J, Zhang L C. Enhanced corrosion and wear resistance properties of carbon fiber reinforced Ni-based composite coating by laser cladding. *Surf Coat Technol* **334**: 274–285 (2018)

[45] Keshri A K, Huang J, Singh V, Choi W, Seal S, Agarwal A. Synthesis of aluminum oxide coating with carbon nanotube reinforcement produced by chemical vapor deposition for improved fracture and wear resistance. *Carbon* **48**(2): 431–442 (2010)

[46] Carpenter C R, Shipway P H, Zhu Y. Electrodeposition of nickel–carbon nanotube nanocomposite coatings for enhanced wear resistance. *Wear* **271**(9–10): 2100–2105 (2011)

[47] Chen X, Zhang G, Chen C, Zhou L, Li S, Li X. Carbon nanotube composite deposits with high hardness and high wear resistance. *Adv Eng Mater* **5**(7): 514–518 (2003)

[48] Sirghi L, Kylián O, Gilliland D, Ceccone G, Rossi F. Cleaning and hydrophilization of atomic force microscopy silicon probes. *J Phys Chem B* **110**(51): 25975–25981 (2006)

[49] Sader J E, Chon J W M, Mulvaney P. Calibration of rectangular atomic force microscope cantilevers. *Rev Sci Instrum* **70**(10): 3967–3969 (1999)

[50] Fujikane M, Setoyama D, Nagao S, Nowak R, Yamanaka S. Nanoindentation examination of yttria-stabilized zirconia (YSZ) crystal. *J Alloys Compd* **431**(1–2): 250–255 (2007)

[51] Dehestani M, Adolfsson E. Phase stability and mechanical properties of zirconia and zirconia composites. *Int J Appl Ceram Technol* **10**(1): 129–141 (2013)

[52] Ru C Q. Effective bending stiffness of carbon nanotubes. *Phys Rev B* **62**(15): 9973–9976 (2000)

[53] Valencia F J, Santiago J, González R I, González-Arrabal R, Ruestes C, Díaz M P, Monclus M A, Molina-Aldareguia J, Nuñez P D, Munoz F, et al. Nanoindentation of amorphous carbon: A combined experimental and simulation approach. *Acta Materialia* **203**: 116485 (2021)

[54] Koumoulos E P, Charitidis C A. Surface analysis and mechanical behaviour mapping of vertically aligned CNT forest array through nanoindentation. *Appl Surf Sci* **396**: 681–687 (2017)

[55] Bokobza L, Zhang J. Raman spectroscopic characterization of multiwall carbon nanotubes and of composites. *Express Polym Lett* **6**(7): 601–608 (2012)

[56] Ferrari A C, Robertson J. Origin of the 1150-cm^{-1} Raman mode in nanocrystalline diamond. *Phys Rev B* **63**(12): 121405 (2001)

[57] Pezzotti G, Camara C, Marin E, Zhu W L, Green D, Collins A, Putterman S. Physical chemistry insights into surface charge phenomena during frictional coupling in triboelectric X-ray sources. *J Mater Chem C* **7**(25): 7708–7724 (2019)

[58] Khadem M, Penkov O V, Jais J, Bae S M, Dhandapani V S, Kang B, Kim D E. Formation of discrete periodic nanolayered coatings through tailoring of nanointerfaces—Toward zero macroscale wear. *Sci Adv* **7**(47): eabk1224 (2021)

[59] Cui W G, Lai Q B, Zhang L, Wang F M. Quantitative measurements of sp^3 content in DLC films with Raman spectroscopy. *Surf Coat Technol* **205**(7): 1995–1999 (2010)

[60] Al Mahmud K A H, Kalam M A, Masjuki H H, Mobarak H M, Zulkifli N W M. An updated overview of diamond-like carbon coating in tribology. *Crit Rev Solid State Mater Sci* **40**(2): 90–118 (2015)

[61] Chung K H, Kim D E. Fundamental investigation of micro wear rate using an atomic force microscope. *Tribol Lett* **15**(2): 135–144 (2003)

[62] Li C X, Liu Y L, Yao X F, Ito M, Noguchi T, Zheng Q S. Interfacial shear strengths between carbon nanotubes. *Nanotechnology* **21**(11): 115704 (2010)

[63] Yu M F, Lourie O, Dyer M J, Moloni K, Kelly T F, Ruoff R S. Strength and breaking mechanism of multiwalled carbon nanotubes under tensile load. *Science* **287**(5453): 637–640 (2000)

[64] Zhang L W, Wang X, Xu W Z, Zhang Y Y, Li Q W, Bradford P D, Zhu Y T. Strong and conductive dry carbon nanotube films by microcombing. *Small* **11**(31): 3830–3836 (2015)

[65] Zhang L W, Ma X L, Zhang Y Y, Bradford P D, Zhu Y T. Length-dependent carbon nanotube film structures and mechanical properties. *Nanotechnology* **32**(26): 265702 (2021)

[66] Jiang K L, Li Q Q, Fan S S. Spinning continuous carbon nanotube yarns. *Nature* **419**(6909): 801 (2002)

[67] Kuzumaki T, Obara Y, Ishiyama Y, Sato R, Takashima M, Ohtake N. Tensile strength of DLC films evaluated by a nanomaterials testing system. *Diam Relat Mater* **25**: 1–4 (2012)

[68] Wilson G M, Sullivan J L. An investigation into the effect of film thickness on nanowear with amorphous carbon-based coatings. *Wear* **266**(9–10): 1039–1043 (2009)

[69] Yoon E S, Singh R A, Oh H J, Kong H. The effect of contact area on nano/micro-scale friction. *Wear* **259**(7–12): 1424–1431 (2005)

[70] Robertson J. Diamond-like amorphous carbon. *Mater Sci Eng R Rep* **37**(4–6): 129–281 (2002)

Kuk-Jin SEO. He received his B.S. degree in Department of Mechanical Engineering from Yonsei University, Seoul, Republic of Korea, in 2014. Currently, he is a Ph.D. candidate at Yonsei University, Seoul, Republic of Korea. His research interests include wear-resistant nanostructured and multi-layered coatings via experimental and computational techniques.

Hyun-Joon KIM. He is an associate professor at Department of Precision Mechanical Engineering at Kyungpook National University, Sangju, Republic of Korea. He received his B.S and Ph.D. degrees in mechanical engineering from Yonsei University, Seoul, Republic of Korea, in 2005 and 2012, respectively. Prof. KIM serves in the editorial board of *Tribology and Lubricants* and *Frontiers* in mechanical engineering. His current interests are the AFM-based nano-mechanics, micro-nano tribology, numerical analysis of tribological behavior, and molecular dynamics simulation.

Dae-Eun KIM. He is a professor at Department of Mechanical Engineering at Yonsei University, Seoul, Republic of Korea. He received his B.S. degree from Tufts University, Medford, USA, and M.S. and Ph.D. degrees from Massachusetts Institute of Technology, Cambridge, USA. Currently, He is a fellow of the Korean Academy of Science and Technology and CIRP. Dr. Kim is also the vice president of Asia Tribology Council and Chair of IFToMM Member Organization for Korea. Dr. Kim serves in the editorial board of several journals including *Tribology Letters* and *Friction*. His research interests are tribology, coatings, and micro-fabrication.